IVYSPRING INTERNATIONAL PUBLISHER

Theranostics

2018; 8(15): 4247-4261. doi: 10.7150/thno.25131

Research Paper

Development and evaluation of a CEACAM6-targeting theranostic nanomedicine for photoacoustic-based diagnosis and chemotherapy of metastatic cancer

Hohyeon Lee[1], Yongho Jang[1], Suhyun Park[1], Hyejin Jang[1], Eun-Joo Park[2], Hyun Jung Kim[3] and Hyuncheol Kim[1,4]✉

1. Department of Chemical & Biomolecular Engineering, Sogang University, #1 Shinsu-dong, Mapo-gu, Seoul, 121-742, Republic of Korea
2. Biomedical Research Institute & Department of Radiology, Seoul National University Hospital, 101 Daehak-ro, Jongno-gu, Seoul, 03080, Republic of Korea
3. Department of Biomedical Engineering, The University of Texas at Austin, Austin, TX 78712, USA
4. Department of Biomedical Engineering, Sogang University, #1 Shinsu-dong, Mapo-gu, Seoul, 121-742, Republic of Korea

✉ Corresponding author: Hyuncheol Kim, Ph.D., Department of Chemical & Biomolecular Engineering, Department of Biomedical Engineering, Sogang University, #35 Baekbeom-ro, Mapo-gu, Seoul 121-742, Republic of Korea. Tel: +82-2-705-8922; Fax: +82-2-3273-0331; E-mail: hyuncheol@sogang.ac.kr

Received: 2018.01.24; Accepted: 2018.07.02; Published: 2018.07.30

Abstract

Metastasis is the leading cause of cancer-related deaths. A number of chemotherapeutic and early diagnosis strategies, including nanomedicine, have been developed to target metastatic tumor cells. However, simultaneous inhibition and imaging of metastasis is yet to be fully achieved.

Methods: To overcome this limitation, we have developed human serum albumin-based nanoparticles (tHSA-NPs) with photoacoustic imaging capability, which target carcinoembryonic antigen-related cell adhesion molecule 6 (CEACAM6). CEACAM6 is highly expressed in metastatic anoikis-resistant tumor cells.

Results: *In vitro*, the CEACAM6-targeting tHSA-NPs efficiently targeted CEACAM6-overexpressing metastatic anoikis-resistant tumor cells. *In vivo*, CEACAM6-targeting tHSA-NPs administered intravenously to BALB/c nude mice efficiently inhibited lung metastasis in circulating anoikis-resistant tumor cells compared to the controls. In addition, anoikis-resistant tumor cells can be successfully detected by photoacoustic imaging, both *in vitro* and *in vivo*, using the intrinsic indocyanine green-binding affinity of albumin.

Conclusion: In summary, the CEACAM6-targeting albumin-based nanoparticles allowed the delivery of drugs and photoacoustic imaging to metastatic anoikis-resistant tumor cells *in vitro* and *in vivo*. Based on the expression of CEACAM6 in a variety of tumors, CEACAM6-targeting nanomedicine might be used to target various types of metastatic tumor cells.

Key words: metastasis, anoikis resistance, CEACAM6, nanomedicine, photoacoustic imaging

Introduction

Tumor metastasis is the most difficult treatment barrier in cancer therapy. Most (up to 90%) cancer-related deaths are a result of metastasis [1]. Metastasized tumors usually become drug-resistant [2, 3], resulting in low survival rates of cancer patients. Therefore, the early detection and treatment of metastasized tumors is very important for maximizing the survival rate and achieving the best prognosis of cancer patients. Various nanomedicines have been developed for efficient and specific treatment of metastatic tumor cells, including nanoparticles (NPs) based on gold [4], magnetic [5], carbon [6], lipid [7], and proteins [8]. However, few satisfactory technologies that simultaneously diagnose and treat cancer cells in the metastatic process or in the early stages of metastasis have been

reported. The reasons are a lack of optimal biomarkers for metastatic tumor cell-targeted nanomedicines and the lack of highly sensitive theranostic nanomedicines for the diagnosis of circulating or early metastasized tumor cells.

Target biomarkers directly related to the mechanism of metastasis are needed. Anoikis resistance, which is defined as anchorage-independent cell survival, is the major prerequisite of tumor metastasis [9, 10] and is also related to drug resistance [8]. During metastasis, tumor cells detach from the primary tumor site to enter the circulatory system, where the cells acquire anoikis resistance that enables tumor metastasis to occur [10-13]. Therefore, targeting circulating anoikis-resistant (AR) tumor cells is one of the best therapeutic strategies to prevent metastasis. A potential biomarker is carcinoembryonic antigen-related cell adhesion molecule 6 (CEACAM6, also known as CD66c). CEACAM6 is closely related to the AR mechanism and to other important metastatic stages, such as migration and invasion, in various types of cancers [11, 14]. Since CEACAM6 is a potential therapeutic target for the treatment of various types of cancers, such as breast [14], pancreatic [15] and lung cancers [16], we selected CEACAM6 as a target biomarker for metastatic AR tumor cells. Based on the aforementioned explanations, a metastasis-specific AR tumor cell-targeting nanomedicine should be capable of inhibiting metastasis and enabling accurate early diagnosis. To achieve this, we selected photoacoustic imaging and human serum albumin (HSA) as the method of diagnosis and the nanomedicine, respectively (**Figure 1**). Photoacoustic imaging, which involves real-time performance, non-invasiveness, and high-resolution imaging [17, 18], has appropriate properties for the imaging of metastatic AR tumor cells. For photoacoustic imaging, we used indocyanine green (ICG), which has an intrinsic affinity to HSA molecules. An HSA molecule possesses avid biocompatibility and abundant functional groups that facilitate the conjugation of CEACAM6 antibodies to the surface of the nanomedicine [19].

In this study, we developed doxorubicin-encapsulated HSA NPs (D@NPs). CEACAM6-targeted nanomedicine (D@C6-NPs) was developed by conjugating anti-CEACAM6 antibodies to the surface of the NPs to target metastatic AR tumor cells. The chemotherapeutic and photoacoustic-based diagnostic ability of the developed CEACAM6-targeting albumin-based nanomedicine was investigated on metastatic AR tumors *in vitro* and *in vivo,* following the intravenous administration of the CEACAM6-targeting nanomedicine. By delivering a high concentration of chemotherapeutic drugs to the circulating metastatic AR tumor cells, formation of metastatic colonies in distant settlement sites could be inhibited. In addition, the CEACAM6-targeting nanomedicine showed successful photoacoustic-based early diagnosis of lung-metastasized AR tumors.

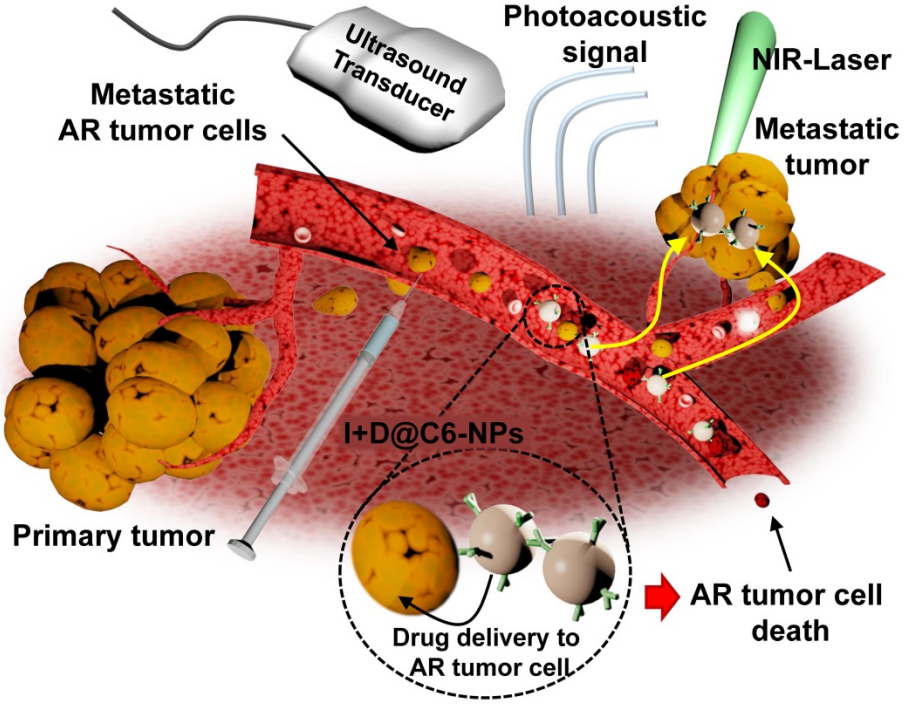

Figure 1. Schematic illustration of a CEACAM6-targeting nanomedicine for simultaneous chemotherapy and photoacoustic imaging of metastatic tumor cells. The intravenously administered CEACAM6-targeting albumin-based nanomedicine can target blood-circulating anoikis-resistant (AR) metastatic tumor cells. Encapsulated doxorubicin (DOX) and indocyanine green (ICG) exhibit inhibition and photoacoustic-based diagnosis of tumor metastasis, respectively.

Methods

Materials

Doxorubicin (DOX), human serum albumin (HSA), 2-iminothiolane hydrochloride (2-IT), ethylenediaminetetraacetic acid (EDTA), 1-ethyl-3-(3-dimethylaminopropyl)carbodiimide (EDC), N-hydroxysuccinimide (NHS), glutathione (GSH), indocyanine green (ICG) and 4-(2-hydroxyethyl)-1-piperazineethanesulfonic acid (HEPES) were purchased from Sigma-Aldrich (Saint Louis, MO, USA). PD-10 desalting columns were purchased from GE Healthcare (Piscataway, NJ, USA). Amicon Ultra-15 centrifugal filter units with a molecular weight cut-off of 30 kDa were purchased from Millipore (Billerica, MA, USA). MCF-7 (HTB-22), MDA-MB-231 (HTB-26), and A549 (CCL-185) tumor cell lines were purchased from American Type Culture Collection (ATCC, Manassas, VA, USA). All other chemicals were of high-performance liquid chromatography (HPLC) grade.

Synthesis of Doxorubicin-encapsulated and CEACAM6-targeting human serum albumin nanoparticles

DOX-encapsulated human serum albumin nanoparticles (D@NPs) were prepared by an ethanol desolvation method. HSA (40 mg) was dissolved in reaction buffer (pH 8.0) containing 1 mM HEPES and 0.1 mM EDTA. Thiolated human serum albumin (tHSA) was prepared by a thiolation process using 2-IT at a range of molar ratios (12.5–37.5) per albumin molecule. After the thiolation process, tHSA was purified using PD-10 desalting columns. The tHSA was concentrated using an Amicon Ultra-15 centrifugal filter unit with a molecular weight cut-off of 30 kDa. Then, ethanol was added in a drop wise manner to the mixture of tHSA and DOX solution in HEPES buffer to produce nano-aggregates of tHSA molecules. After overnight reaction, D@NPs in the reaction solution were harvested by centrifugation at 16,100 × *g* for 10 min to eliminate ethanol and other unreacted impurities. Finally, the re-suspended tHSA-NPs were centrifuged at 800 × *g* for 5 min to eliminate micro-sized particles. The fabrication of empty NPs proceeded in exactly the same way except that the addition of DOX was omitted. To prepare CEACAM6-targeting D@NPs (D@C6-NPs), CEACAM6 antibodies (Sigma-Aldrich) were conjugated to the surface of tHSA-NPs via NHS/EDC chemistry in MES reaction buffer (Thermo Fisher Scientific, Waltham, MA, USA) as depicted in **Figure 3A**. After allowing the reaction to proceed for 15 min at 25 °C, NHS/EDC-activated antibodies were purified using a centrifugal filter. The activated antibodies were mixed with the D@NP solution *in situ* and amide bonding between the antibody molecules and NPs occurred for 1.5 h. Finally, a purification process (centrifugation at 16,100 × *g* for 10 min) was carried out to purify the D@C6-NPs from the unreacted materials in the solution.

Conjugation of indocyanine green (ICG) to the CEACAM6-targeting albumin-based nanomedicine

ICG was non-covalently conjugated to the surface of the developed albumin-based nanomedicine for photoacoustic imaging. ICG binding was conducted before the conjugation of CEACAM6 antibody. ICG in distilled water (1 mg/mL) was incubated at 37 °C for more than 2 h for complete dissolution. The ICG solution (100 µL) was added to 1 mL of the nanomedicine solution. After overnight incubation at 25 °C, unreacted ICG was removed by centrifugation at 16,100 × *g* for 10 min. The absorbance spectrum and entrapment efficiency of the ICG-conjugated D@C6-NPs (I+D@C6-NPs) was measured by ultraviolet/visible (UV/Vis) spectrophotometry (Thermo Fisher Scientific).

Photoacoustic imaging

For photoacoustic imaging, laser light irradiation at a wavelength of 780 nm was supplied using the Q-switch trigger of an Nd:YAG laser excitation system (Surelite III-10 and Surelite OPO Plus, Continuum Inc., Santa Clara, CA, USA) through a custom-built fiberoptic bundle (Fiberoptic Systems Inc., Simi Valley, CA, USA). The laser intensity was 7 mJ/cm^2. For *in vitro* photoacoustic imaging, a water-immersed Tygon® tube (0.04-inch internal diameter) was used to contain the sample solution. A conventional ultrasound transducer with an operating frequency range of 4–7 MHz was used to receive photoacoustic signals. The acquired data was imaged through MATLAB® software (MathWorks, Natick, MA, USA). For *ex vivo* photoacoustic imaging, the same settings were used, except that the lungs were placed directly in a water bath. *In vivo* lung photoacoustic imaging was performed using the Vevo LAZR Imaging System (FUJIFILM VisualSonics, Inc., Toronto, ON, Canada). Laser light (780 nm) was delivered through the fiberoptic bundles integrated into an ultrasound transducer (LZ550, f_c = 50 MHz). For photoacoustic contrast stability testing, ICG-conjugated tHSA-NPs (I@NPs) and ICG-conjugated D@NPs (I+D@NPs) were suspended in either 1× phosphate buffered saline (PBS) or 50% fetal bovine serum. After 24 h, photoacoustic signals from purified (centrifugation at 16,100 × *g* for 10 min) and re-suspended I@NPs and I+D@NPs were evaluated with the same concentration of free ICG.

Characterization of CEACAM6-targeting and Doxorubicin-encapsulated tHSA-NPs (D@C6-NPs)

The size and shape of the fabricated NPs were determined using a Zetasizer (Nano-ZS; Malvern Instruments, Malvern, UK) and transmission electron microscopy (TEM), respectively. The entrapment efficiency of DOX in the NPs corresponding to the thiolation ratio was determined using HPLC. Samples (100 µL) were injected with an autosampler (YL9150; Younglin Inc., Seoul, South Korea). A 250 × 4.6 mm (5 µm) ZORBAX Eclipse Plus C18 column (Agilent Technologies, Santa Clara, CA, USA) was used for separation. DOX concentrations were monitored at 254 nm using a model YL9120 UV detector (Younglin Inc.). The retention time was 6 min. For *in vitro* release study, free DOX, D@NPs, and ICG-conjugated D@NPs (I+D@NPs) were placed in dialysis membrane tubes (molecular weight cut-off of 2 kDa). The dialysis membrane tubes were immersed in 10 mL of PBS and replaced at each time point. The concentration of DOX at each time point was also determined using HPLC. To confirm the conjugation of CEACAM6 antibodies to the surface of the NPs, goat anti-rabbit IgG antibodies (Alexa Fluor 488-conjugated) were used to visualize the CEACAM6 antibodies. NPs were also visualized using Alexa Fluor 555-NHS ester. Two-channel images were obtained using laser scanning confocal microscopy (TCS SP8; Leica Microsystems, Wetzler, Germany).

Cell culture

MCF-7 and MDA-MB-231 human breast tumor cells and A549 human lung tumor cells were cultured in Dulbecco's modified Eagle's medium (GibcoBRL, Grand Island, NY, USA) supplemented with 10% fetal bovine serum (GibcoBRL). Adherent cells were cultured in a tissue culture dish (Falcon, San Jose, CA, USA), while suspension cultures were grown in dishes coated with 10 mg/mL poly(2-hydroxyethyl methacrylate) (poly-HEMA, Sigma-Aldrich). To select cells that could survive in suspension culture, 1×10^6 cells were seeded onto poly-HEMA-coated dishes and incubated for more than a week for use in further experiments. Fresh medium was added every three days. After seven days in culture, cells were harvested and treated with diluted trypsin-EDTA to obtain a single-cell suspension for re-plating or Trypan blue dye exclusion assays.

CEACAM6 expression in AR human tumor cells

Harvested cells were pelleted and re-suspended in 500 µL of PBS. Cells were fixed with 3.7% paraformaldehyde (PFA), permeabilized, and blocked using a buffer solution containing PBS, bovine serum albumin, Triton, and azide (PBTA). The cells were incubated with rabbit anti-human CEACAM6 antibodies. After incubation for 1 h at 25 °C, the cells were rinsed with 1× PBS and incubated with goat anti-rabbit IgG (Alexa Fluor 488-conjugated) for 30 min at 25 °C. The cells were counterstained using a mounting medium containing 4',6-diamidino-2-phenylindole (DAPI) and imaged at appropriate wavelengths using a fluorescence microscope. Reverse-transcription polymerase chain reaction (RT-PCR) and quantitative real-time PCR were used to analyze the CEACAM6 mRNA expression in both adherent and AR cells. The following CEACAM6 primers were purchased from Bioneer (Daejeon, South Korea): CEACAM6 forward, 5′-TACTCAGCGT CAAAAGGAAC-3′; CEACAM6 reverse, 5′-AGAGAC TGTGATCATCGTGA-3′. The results of RT-PCR were analyzed by gel retardation assay, in which ethidium bromide-stained bands were visualized by a Gel Doc imaging device (Bio-Rad, Richmond, CA, USA).

Intracellular distribution of C6-NPs and *in vitro* photoacoustic imaging

The intracellular distribution of the empty CEACAM6-targeting tHSA-NPs (C6-NPs) was analyzed by laser scanning confocal microscopy (TCS SP8; Leica Microsystems). A549 and A549 AR cells (5×10^5 per well) were seeded in 12-well cell culture dishes coated with poly-HEMA. Cells were treated with Alexa Fluor 555-conjugated tHSA-NPs and C6-NPs at 37 °C. After incubation for 30 min with gentle shaking, the cells were collected, washed using 1× PBS, and fixed with 3.7% PFA for 10 min. After fixation, the cells were incubated with a 1:40 dilution of Alexa Fluor 488 phalloidin (Invitrogen, Carlsbad, CA, USA) for 30 min to stain F-actin and washed with PBTA buffer. The cells were mounted with mounting medium containing DAPI. LAS AF (Leica Microsystems) and Volocity (PerkinElmer, Waltham, MA, USA) software were used to analyze the obtained images. For *in vitro* photoacoustic imaging, ICG-conjugated C6-NPs (I@C6-NPs) and I@NPs were incubated with A549 AR cells for 6 h with shaking. After incubation, A549 AR cells were centrifuged and washed several times. Finally, A549 AR cells were concentrated to 1×10^5 to 1×10^6 cells/mL. L7_4 array transducer and Verasonics ultrasound system (Verasonics, Redmond, WA) were used to receive *in vitro* photoacoustic signals.

In vitro cell viability

Cell viability was determined by the Trypan blue dye exclusion method. Both adherent and A549 AR cells were seeded in 6-well plates. The cells were incubated with medium containing 100 nM DOX and

the quantity of NPs corresponding to the entrapped DOX was calculated. After 6 h of incubation under static or shaking conditions, the medium was replaced with fresh medium and the cells were incubated for 72 h. Cell viability was determined by incubating the cells with 0.4% Trypan blue dye and counting the viable cells using a Neubauer hemocytometer.

Metastasis animal model and *in vivo* experiments of therapy, and *ex vivo* and *in vivo* photoacoustic imaging

To evaluate active targeting and the efficiency of drug delivery of D@C6-NPs *in vivo,* twenty BALB/c nude mice were divided randomly into four groups (five per group). The mice were housed in 12-h cycles of light and dark with unrestricted access to food and water. After adaptation for more than a week, 2×10^6 A549 AR cells were injected into the tail vein of each mouse. The treatment was conducted twice in each group. The first treatment was immediately performed after the injection of the metastatic AR cells and the second treatment was performed four days later (10 mg DOX/kg body weight). The body weights of the mice were recorded every second day. On day 16, the mice were euthanized and their lungs were harvested for the analysis of metastasized tumor colonies. The harvested lungs were stained with Bouin's solution to clearly visualize the metastasized tumor regions. After 24 h, images of tumor colonies were captured and analyzed by Image-Pro Plus software (Media Cybernetics, Inc., Rockville, MD, USA). The contrast of the images of lungs stained with Bouin's solution was enhanced for the best visualization of tumor colonies. Clear metastatic nodules were counted and quantified. Major organs were explanted for histological analysis. The organs were embedded in paraffin blocks and sectioned into 5-μm-thick slices. The sectioned tissue slices were stained with hematoxylin and eosin. For *ex vivo* lung photoacoustic imaging, 1.5×10^6 A549 AR cells were injected into the tail vein of each mouse (N = 3). After two weeks, I@NPs and I@C6-NPs were intravenously injected and the lungs were harvested 6 h after the injection. The lungs were immersed in a water bath and photoacoustic imaging was performed with the same process as the *in vitro* photoacoustic imaging experiments. For *in vivo* photoacoustic imaging, the same conditions were used. Twenty-four hours after NP injection, the mice (N = 3) were anesthetized and the lungs were imaged using a VisualSonics Vevo LAZR-2100 device equipped with a 40-MHz transducer. All animal experiments were performed in accordance with the guidelines of the Sogang University Animal Studies Committee.

Data analysis

All data were compiled from a minimum of three replicate experiments. Data are expressed as the mean ± standard deviation. Statistical analysis was performed using Student's t-test and one-way ANOVA for multiple comparisons. The difference between two groups was considered statistically significant at $p \leq 0.05$.

Results

Characteristics of nanoparticles (NPs)

The tHSA-NPs fabricated with disulfide cross-linking showed an average diameter of 188.4 ± 4.0 nm (PDI: 0.16 ± 0.02), which did not depend on drug encapsulation (**Figure 2A** and **Figure S1A**). TEM images demonstrated the spherical and uniform shape of all NPs (**Figure 2A**). tHSA-NPs were prepared with different degrees of thiolation (12.5-, 25-, or 37.5-fold molar ratio of 2-IT per albumin molecule). D@NPs prepared with a 1:25 thiolation ratio displayed the highest drug capsulation efficiency at 61.1 ± 1.1%. The tHSA-NPs fabricated with thiolation ratios of 1:12.5 and 1:37.5 displayed 19.6% and 16.9% encapsulation efficiency, respectively (**Figure S1B**). Therefore, the D@NPs with a thiolation ratio of 1:25 were used in subsequent experiments because of the highest efficient drug encapsulation and NP production. The *in vitro* release of DOX from the tHSA-NPs was also investigated to determine its release profile (**Figure 2B**). In the first 6 h, almost 70% of the DOX was released. Based on the position of the DOX molecule inside the NPs, it was expected that DOX present near the inner surface of the particles would be rapidly released by initial diffusion, with the remaining drug released gradually. Furthermore, ICG conjugation did not affect the release of DOX from the NPs. The absorbance spectrum of I@NPs displays a slight red-shift pattern compared with that of free ICG, which was caused by the concentration of ICG in tHSA-NPs (**Figure 2C**). This result indicates the successful encapsulation of ICG into the tHSA-NPs. I@NPs displayed sufficient photoacoustic contrast ability (**Figure 2D**). Furthermore, we also confirmed the stability of photoacoustic contrast ability of I@NPs for multiple laser irradiations (**Figure S10**).

Surface modification with antibody conjugation

Human CEACAM6 antibodies were conjugated onto the surface of tHSA-NPs to target circulating metastatic AR tumor cells. **Figure 3A** demonstrates the overall procedure for the conjugation of the antibody onto the surface of tHSA-NPs via the

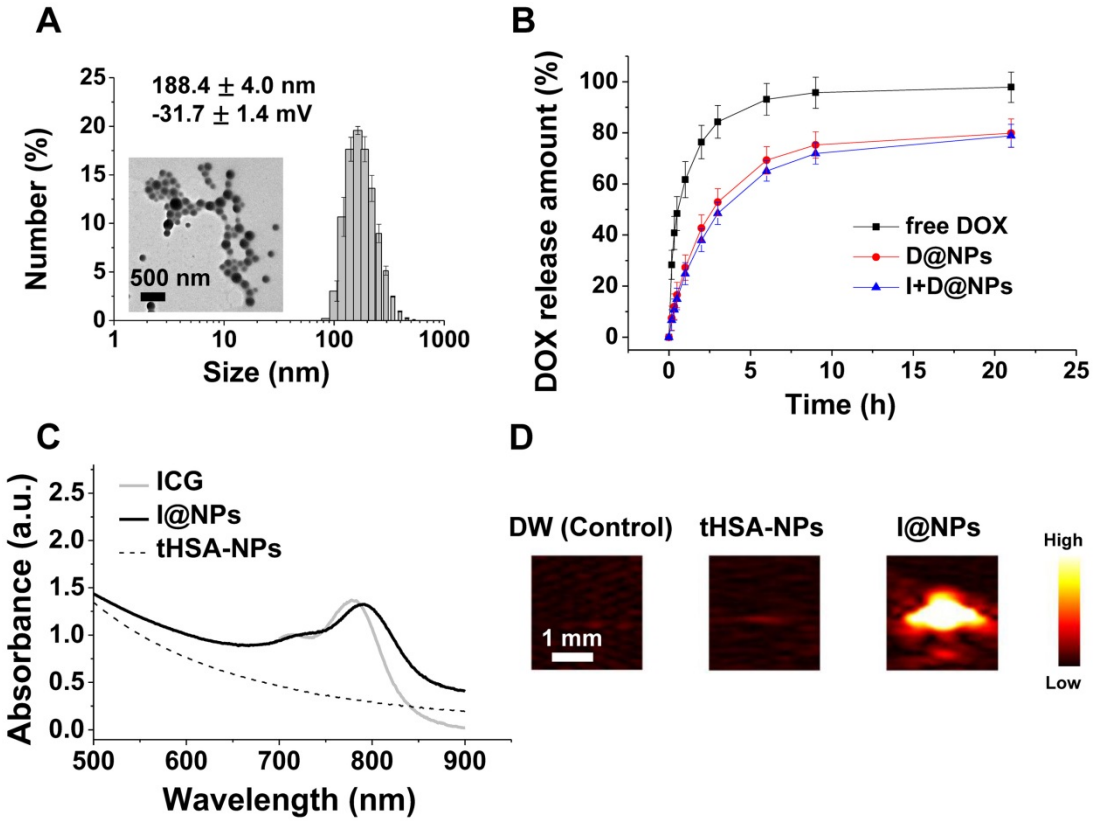

Figure 2. Characteristics of tHSA-NPs with DOX and ICG. (A) Average size and transmission electron micrograph. **(B)** *In vitro* release pattern of DOX-loaded tHSA-NPs (D@NPs). **(C)** Optical absorption spectrum of ICG-conjugated tHSA-NPs (I@NPs) with control groups. **(D)** Photoacoustic signal intensities of tHSA-NPs and I@NPs with control groups. L7_4 transducer (focal depth: 3 cm) was used to obtain *in vitro* photoacoustic images.

EDC/NHS coupling process between the antibody and albumin molecules. Antibody conjugation slightly increased the average diameter of NPs from 241.4 ± 3.8 nm to 260.6 ± 3.5 nm (**Figure 3B**). Immunohistochemistry was performed to visualize the conjugation of the CEACAM6 antibody onto the surface of the NPs. The procedure revealed the co-localization of the secondary antibodies targeting the CEACAM6 antibodies with the NPs (**Figure 3C**, right column). Conversely, no co-localization was observed in the control tHSA-NPs (no conjugation of CEACAM6 antibody) (**Figure 3C**, left column). Therefore, the successful conjugation of CEACAM6 antibodies onto the NPs was confirmed.

Overexpression of CEACAM6 in AR tumor cells

The protein and mRNA expression levels of CEACAM6 were evaluated in the three metastatic AR tumor cell lines by immunohistochemistry and RT-PCR, respectively, and were compared with those of normal adherent tumor cells. Immunohistochemical staining indirectly demonstrated the higher expression of CEACAM6 protein in metastatic MCF-7 AR, MDA-MB-231 AR, and A549 AR tumor cells, compared to that in the adherent tumor cells (**Figure 4A**). Similarly, a higher expression of CEACAM6 mRNA was evident in metastatic AR tumor cells compared to that in the adherent tumor cells (**Figure 4B**). Quantitative real-time RT-PCR revealed that MCF-7 AR, MDA-MB-231 AR, and A549 AR cells expressed 7-, 2-, and 4-fold higher CEACAM6 mRNA, respectively, than their parental adherent tumor cells (**Figure 4C**). The overexpression of CEACAM6 was maintained for up to three days after the re-attachment of formerly detached AR-induced tumor cells (**Figure 4D**).

In vitro intracellular uptake and targeting ability of CEACAM6-targeting tHSA-NPs

The intracellular delivery and targeting ability of the CEACAM6-targeting tHSA-NPs (C6-NPs) were evaluated by fluorescence microscopy (**Figure 5A**) and flow cytometry (**Figure 5B**) in AR and adherent A549 tumor cell lines. In normal adherent tumor cells, both tHSA-NPs (**Figure 5A**, row 1) and C6-NPs (**Figure 5A**, row 2) displayed lower targeting abilities, with no difference in the targeting abilities between the two types of NPs (targeting and non-targeting NPs). C6-NPs demonstrated higher targeting ability in A549 AR tumor cells (**Figure 5A**, row 4) than did tHSA-NPs (**Figure 5A**, row 3) within 30 min, indicating the efficient CEACAM6-targeting ability of the C6-NPs. Flow cytometric analysis also showed

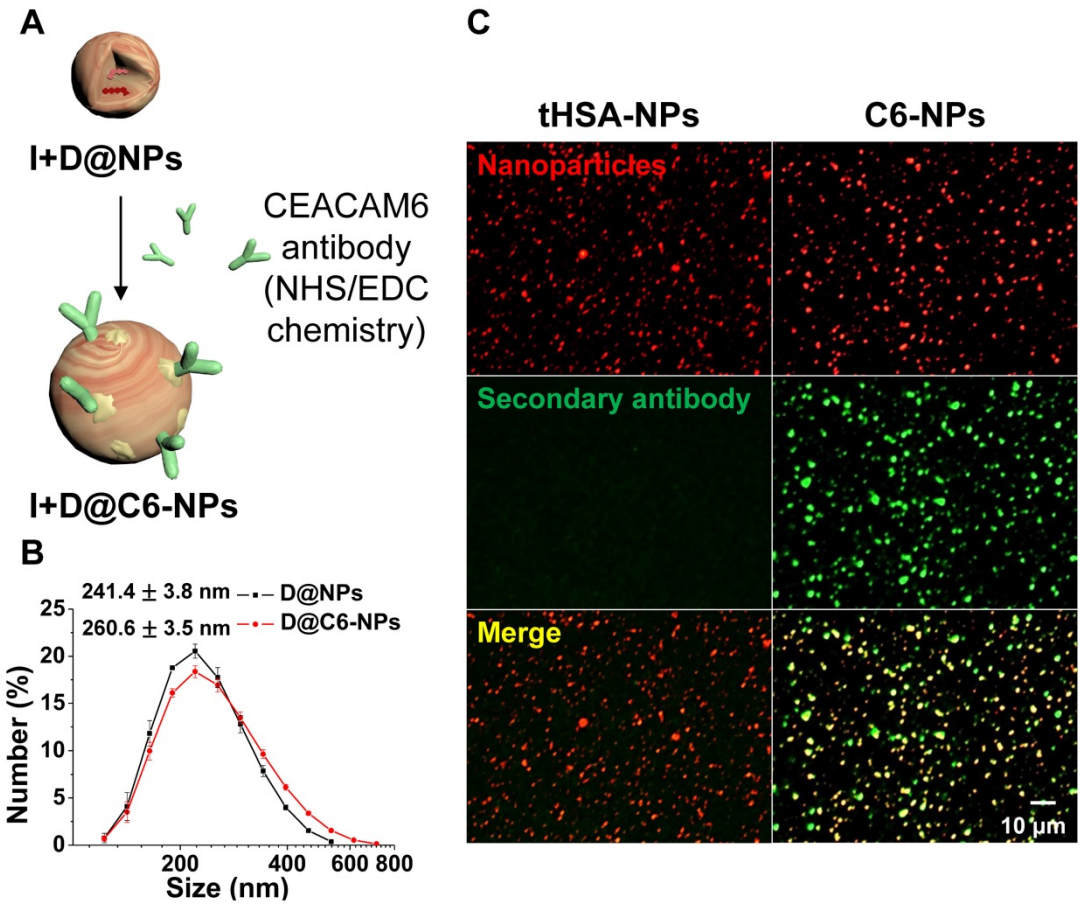

Figure 3. (A) Illustration of CEACAM6 antibody conjugation onto the surface of tHSA-NPs. **(B-C)** Size distribution and immunofluorescence patterns with secondary antibody of nanoparticles before and after antibody conjugation.

similar results. Although the fluorescence spectrum of C6-NPs shifted slightly to the right compared to that of the tHSA-NPs, the difference between the two groups in adherent cells was negligible. However, in AR tumor cells, the fluorescence spectrum of C6-NPs shifted to the right and had a value that was > 20% higher (gated population of 76.23%) than that of tHSA-NPs (gated population of 54.67%). Therefore, the targeting ability of C6-NPs toward metastatic AR tumor cells was confirmed *in vitro*.

In vitro therapeutic efficiency of doxorubicin-encapsulating and CEACAM6-targeting tHSA-NPs against AR tumor cells

An *in vitro* cytotoxicity assay was performed to confirm the targeting ability and chemotherapeutic effect of DOX-encapsulating and CEACAM6-targeting tHSA-NPs (D@C6-NPs) on A549 AR tumor cells. The overall viabilities of cells treated with DOX-encapsulating, non-targeting tHSA-NPs (D@NPs) and DOX-encapsulating, CEACAM6-targeting tHSA-NPs (D@C6-NPs) were decreased compared to those of the control and tHSA-NPs (NPs without any encapsulated chemotherapeutic agent) ($p < 0.05$) in both adherent and AR tumor cells (**Figure 6**). Furthermore, treatment with D@C6-NPs produced higher toxicity in AR tumor cells than did D@NPs ($p < 0.05$) because of their targeting ability. In adherent tumor cells, however, there was no significant difference between treatment with D@NPs and D@C6-NPs ($p > 0.05$). These results are comparable to the data obtained from intracellular uptake and targeting studies (**Figure 5**). In addition, the overall viability of AR tumor cells was higher than that of the adherent tumor cells, indicating the chemoresistance of AR tumor cells (**Figure 6**). The collective results presented in **Figure 5** and **Figure 6** indicated that D@C6-NPs had excellent targeting and drug delivery properties to metastatic AR tumor cells.

Inhibition of metastasis in animal model and immunoassay of metastasized lungs

The targeting ability and therapeutic activity of D@C6-NPs were evaluated in the xenograft metastasis mouse model after intravenous injection. **Figure 7A** shows representative images of metastasized tumor colonies in the enucleated lungs from each group (no injection (CTL); free DOX injection (DOX); D@NPs; D@C6-NPs). Irregularly shaped metastasis nodules

were clearly evident in the front and back of the lungs, and macroscopically detectable nodules were quantified (**Figure 7B**). Lung metastasis was significantly lower in mice treated with D@C6-NPs compared to that observed in untreated control mice and mice treated with free DOX and D@NPs (all $p < 0.01$). In the D@C6-NP-treated group, metastasis was 7.4- and 16.0-fold lower than that in the free DOX and control groups, respectively, based on the number of metastasis nodules. During the experimental period, mice treated with free DOX showed slight body weight loss, indicating the toxicity of the chemotherapeutic agent. However, mice injected with D@NPs or D@C6-NPs showed no significant changes in body weight during the treatment period, demonstrating that the severe toxicity of chemotherapeutic agents can be overcome through the novel nanomedicine (**Figure 7C**). Histological analysis also revealed that there were no significant structural changes in tissue morphology (**Figure 7D**). In addition to the ability of D@C6-NPs to target circulating metastatic tumor cells, the targeting possibility of the nanomedicine to an early-stage metastatic tumor was also investigated with the expression of CD31, an immunohistochemical marker of endothelial trans-differentiation. The expression of CD31 was confirmed, indicating the access of circulating C6D-tHSA-NPs to early-stage metastatic tumor cells through developed tumor angiogenesis (**Figure S2**). In addition, the expression of CEACAM6 in metastatic re-attached tumor cells was confirmed *in vivo* (**Figure S2**), demonstrating the targeting of D@C6-NPs to an early-stage metastatic tumor cells.

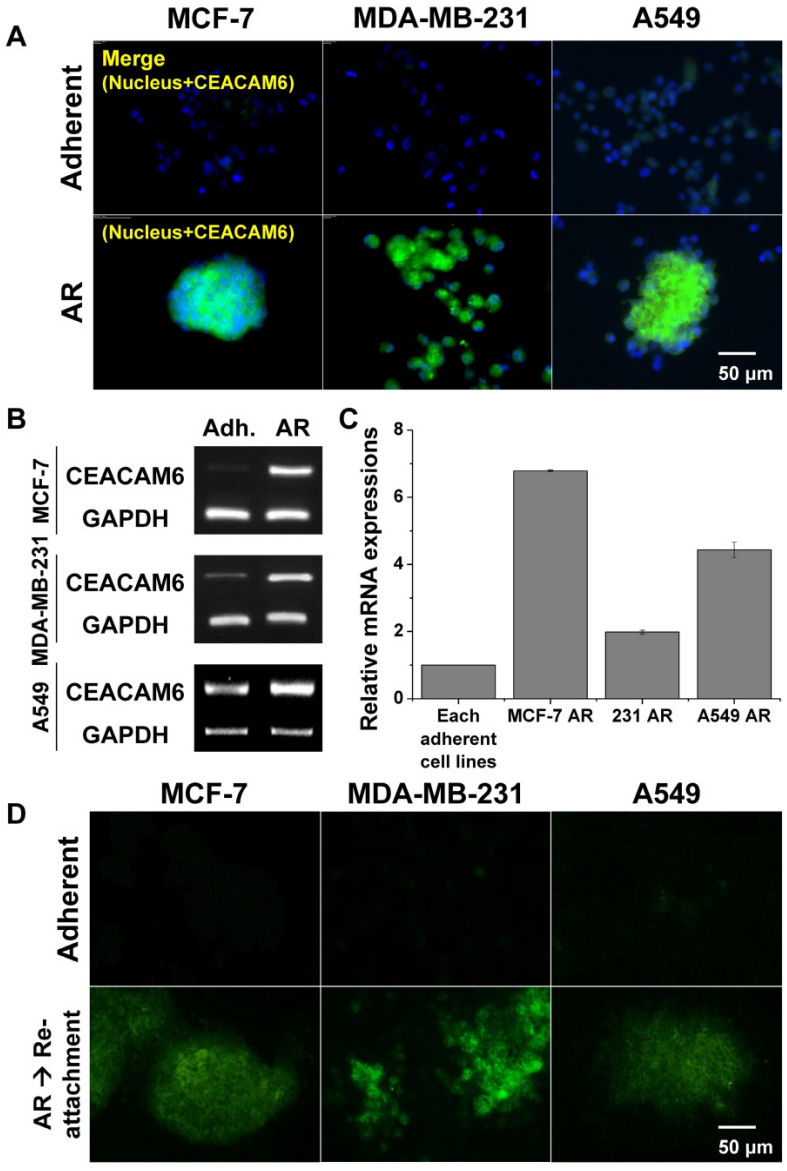

Figure 4. (A) CEACAM6 overexpression in AR tumor cells (MCF-7, MDA-MB-231 and A549). Immunofluorescence of CEACAM6 protein. **(B-C)** CEACAM6 mRNA expressions in three cell lines and its quantification from RT-PCR and real-time RT-PCR. **(D)** CEACAM6 protein expression lasted for 3 days after re-attachment of AR tumor cells in all cell lines.

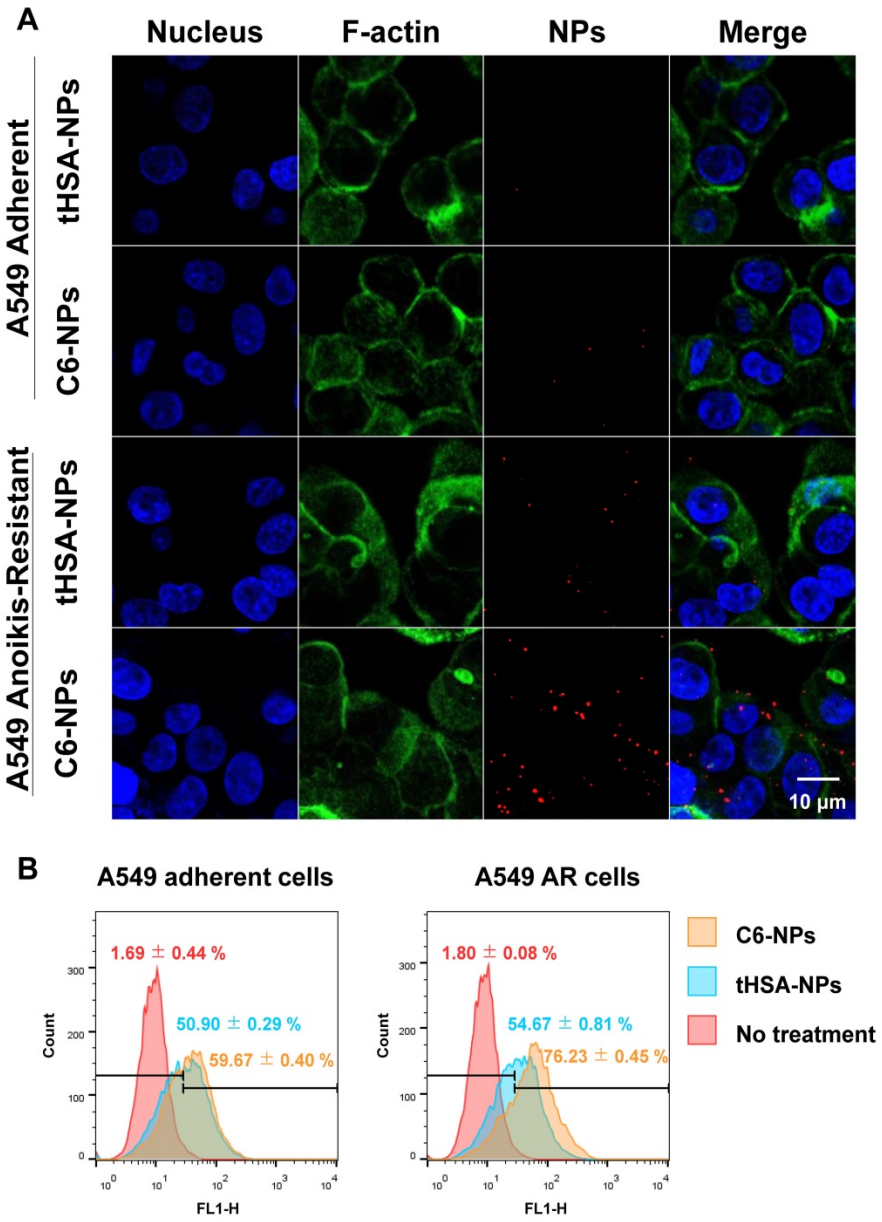

Figure 5. (A) Cellular targeting of CEACAM6-targeting tHSA-NPs (C6-NPs) to A549 adherent and A549 AR cells during shaking for 30 min. Cell nucleus, F-actin and nanoparticles are shown as blue, green, and red, respectively. The rightmost column depicts merged images of all. **(B)** Flow cytometry data for quantification of cellular targeting in the same condition.

Photoacoustic imaging-based diagnosis of an early-stage metastatic tumor with the CEACAM6-targeting nanomedicine

To evaluate the photoacoustic imaging-based diagnosis ability of the CEACAM6-targeting nanomedicine in an early-stage metastatic tumor, two types of NPs were incubated with A549 AR cells for 6 h under gentle shaking. One of them is ICG (photoacoustic imaging contrast agent)-conjugated and CEACAM6-targeting tHSA-NPs (I@C6-NPs), and the other is ICG-conjugated but non-CEACAM6-targeting tHSA-NPs (I@NPs). Photoacoustic signals from I@C6-NP-treated cells were higher than those observed in I@NP-treated cells at all cell concentrations (**Figure 8A**). The quantitative analysis of the photoacoustic signals in each group is shown in **Figure 8B**, indicating the potential of I@C6-NPs in diagnosing an early-stage metastatic tumor. In the *in vivo* metastatic animal model (N = 3), photoacoustic signals from the metastasized lung in the I@C6-NP-treated group were determined to be stronger than those observed in the I@NPs group (**Figure 8C**). For the quantitative analysis, only the photoacoustic signals in the lung were considered by excluding off-targeting of the nanomedicine and noise from certain internal molecules, such as melanin and blood. Figure 8D demonstrates that the photoacoustic signals from the lung in the I@C6-NP-treated group was 2.5-fold higher than those in the I@NP group. For

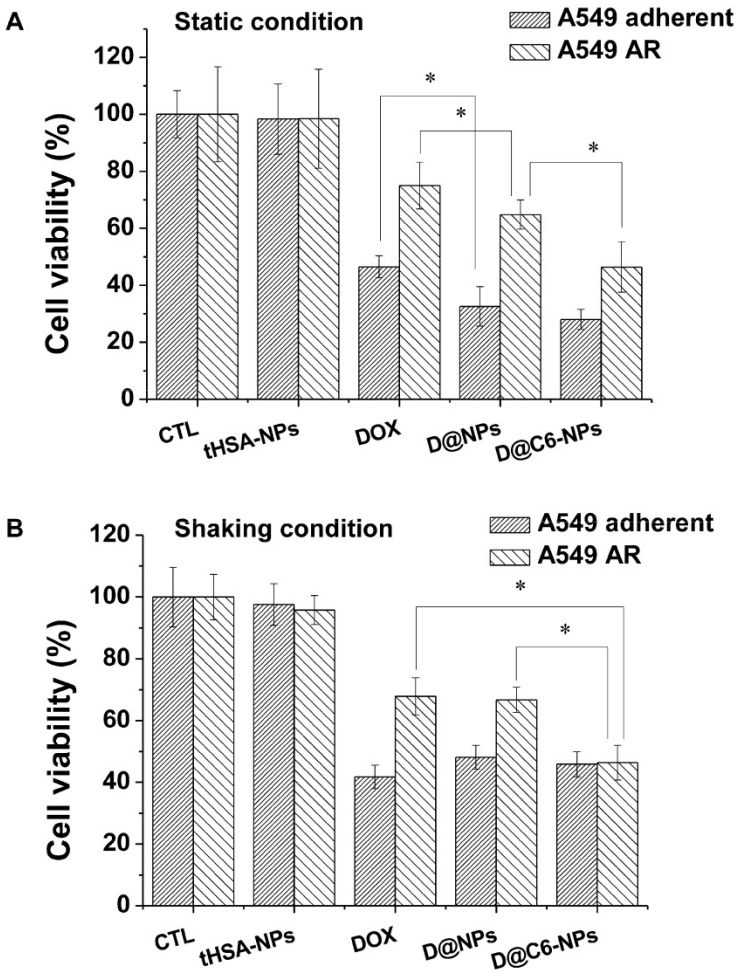

Figure 6. Cell viability assay with parental A549 adherent and A549 AR cells. Cells were treated at a concentration corresponding to 100 nM DOX for 6 h under **(A)** static and **(B)** shaking condition, and further cultured up to 72 h in fresh medium. Bar with dense line and sparse line represent A549 adherent and A549 AR cells, respectively. Asterisk (*) denotes $p<0.05$ between two groups.

a more detailed analysis, the lungs were excised 6 h after the injection under the same experimental conditions, and the photoacoustic signals were analyzed *ex vivo* (**Figure 8E**), demonstrating the high targeting ability of the CEACAM6-targeting NP toward metastatic tumors.

Discussion

In this study, CEACAM6-targeting nanomedicine was developed to efficiently target both circulating and early-stage metastatic AR tumor cells (**Figure 1**). The CEACAM6-targeting and chemotherapeutic agent-encapsulating nanomedicine was found to target metastatic AR cells efficiently and inhibit metastasis to the lung (**Figure 7**). In addition, the CEACAM6-targeting and ICG-loading nanomedicine showed the promise of photoacoustics-based diagnosis in early-stage metastasis (**Figure 8**). HSA molecules were self-aggregated to form NPs using an ethanol desolvation method and were then cross-linked and stabilized via disulfide bonding (tHSA-NPs), instead of adding a chemical cross-linking agent, such as glutaraldehyde, which causes undesired side effects [20]. The photoacoustic agent, ICG, can be efficiently conjugated to the surface of tHSA-NPs with intrinsic affinity to HSA molecules [19]. The chemotherapeutic agent, DOX, was efficiently entrapped in the space between the disulfide bond-cross-linked albumin molecules and in the drug binding sites within the albumin molecules [21]. Because the disulfide bonds were destroyed in the cytoplasmic reduction conditions (**Figure S7**), the tHSA-NPs that have been taken up intracellularly may break down into individual albumin molecules and effectively release the encapsulated chemotherapeutic agent inside the tumor cells [22]. In the *in vitro* release study, 35% of the encapsulated drug was released within 30 min (**Figure 2**). Considering that humans have an average blood circulation time of < 1 min [23], the drug release time is sufficient for NPs to target and kill metastatic tumor cells without significant drug loss (**Figure 6** and **Figure 7**). Consequently, the CEACAM6-targeting and DOX-encapsulating tHSA-NPs successfully

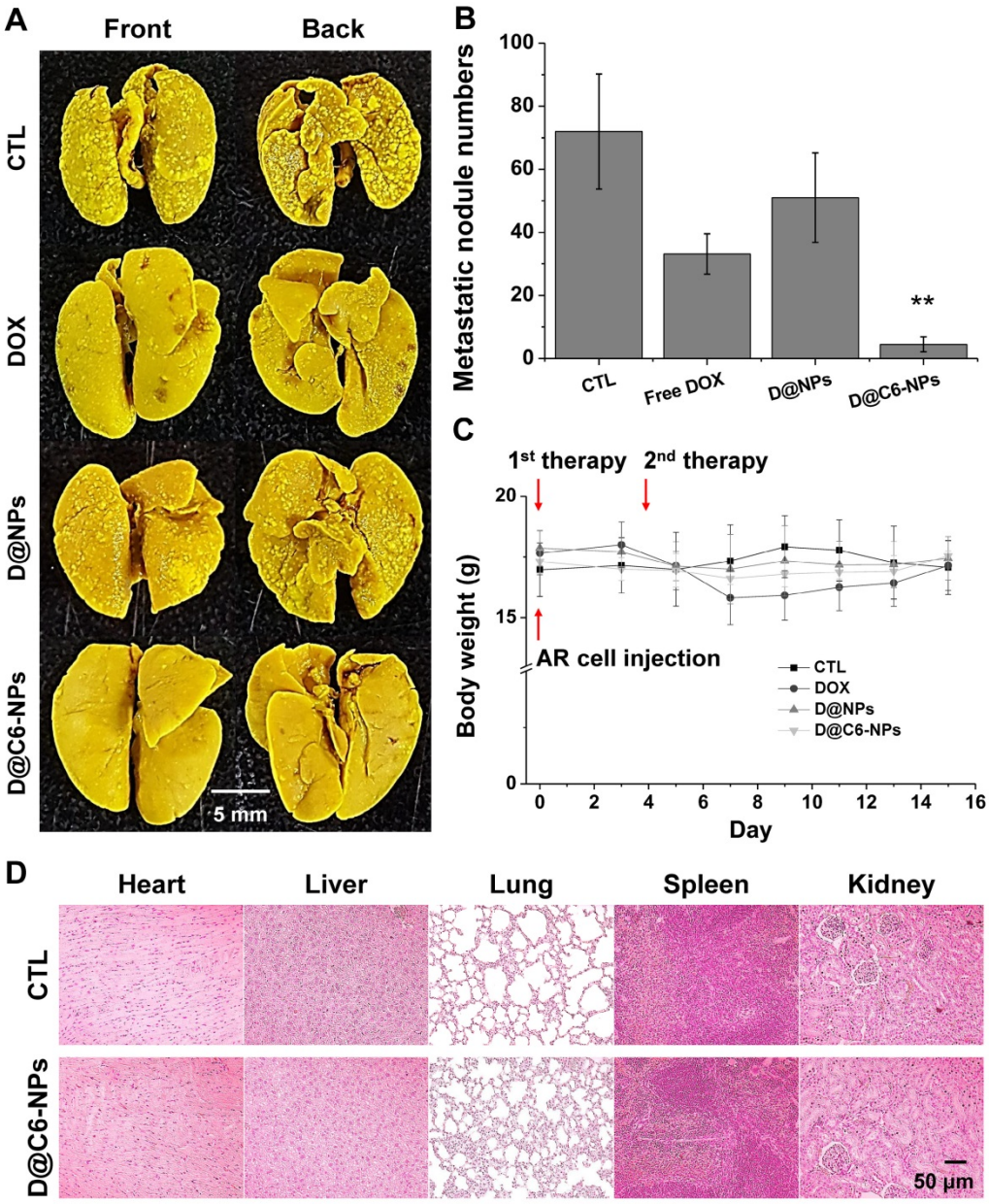

Figure 7. (A-B) *In vivo* metastasis inhibition of D@C6-NPs and other groups. Right after the intravenous injection of A549 AR cells, the first therapy was conducted. After 3 days, the second therapy was performed. Metastatic nodules in BALB/c nude mouse lungs were photographed and the number of metastatic nodules was quantified. D@C6-NPs group displayed statistical significance (ANOVA, $p<0.01$). **(C)** Body weights of mice were recorded at the indicated times. **(D)** H&E analysis of major organs in control and D@C6-NPs groups.

targeted and delivered chemotherapeutic agents to the metastatic tumor cells.

AR tumor cells are highly suitable as a metastatic tumor model because tumor cells must acquire AR property in order to survive in the bloodstream and achieve an active metastatic process [9]. The expression of CEACAM6 was known to be increased when tumor cells were detached from the extracellular matrix (**Figure 4**) [12, 24, 25]. CEACAM6 also plays an important role in events related to metastasis including tumor cell migration, invasion, and adhesion [11]. These roles are not limited to any specific cancer and CEACAM6 is highly overexpressed in many types of metastasizing tumor cells, including breast [14], gastric [26], colorectal [27] and pancreatic cancers [10, 12]. In this study, the overexpression of CEACAM6 in three types of tumor cells (A549 lung tumor cell, MCF-7, and MDA-MB-231 breast tumor cells) was also confirmed (**Figure 4**). Therefore, CEACAM6 can be a good target for metastatic AR tumor cell-specific treatment in various types of cancers. In the *in vitro* study, the targeting and drug delivery efficiency of the CEACAM6-targeting nanomedicine was found to be improved (**Figure 5**, **Figure 6**, **Figure S4**, and **Figure S5**) compared to those of the non-targeting nanomedicine.

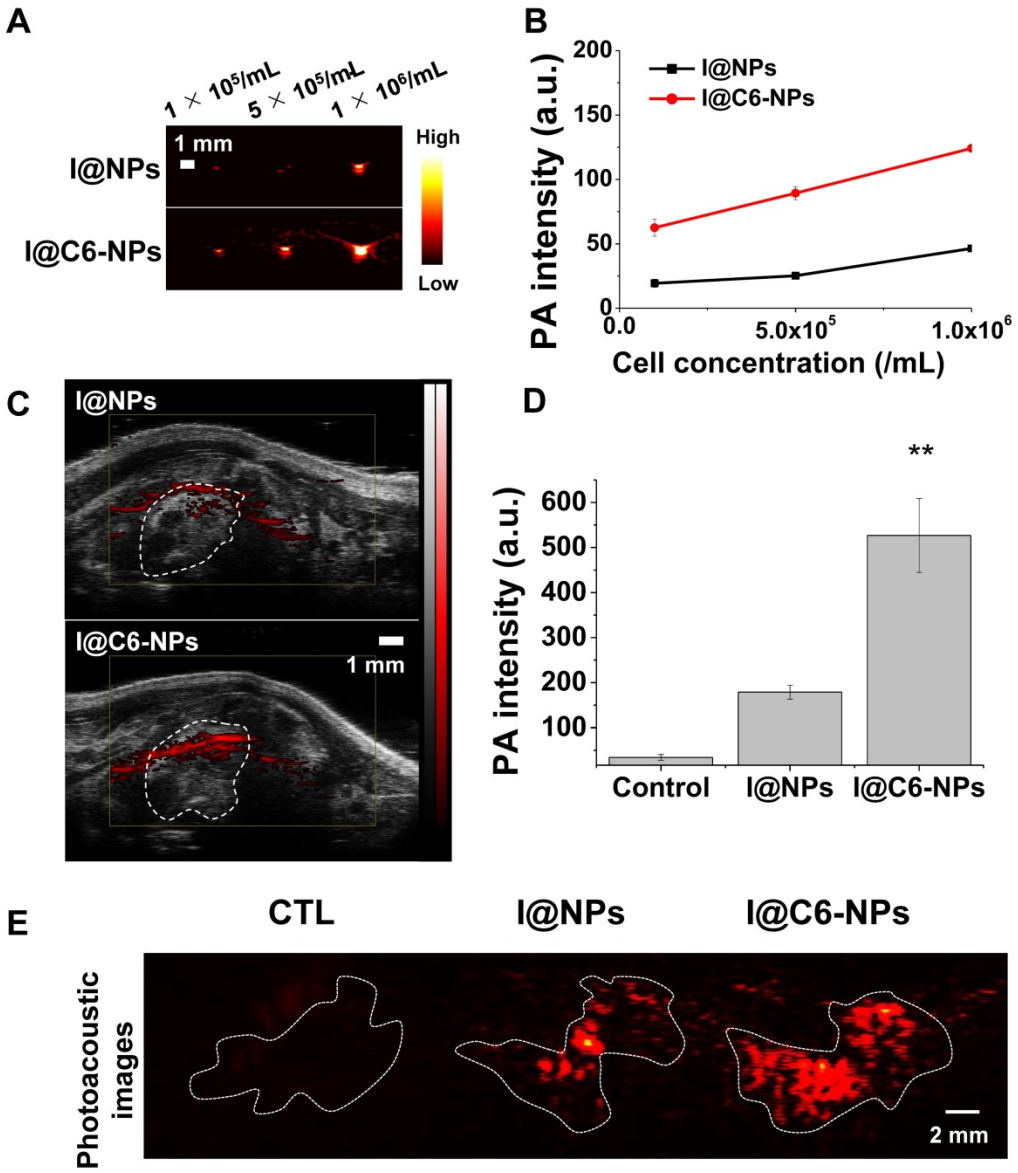

Figure 8. (A-B) *In vitro* and *in vivo* photoacoustic contrast ability of I@C6-NPs. Photoacoustic signals from A549 AR cells after 6 h incubation with I@NPs and I@C6-NPs under shaking conditions and the quantification data. L7_4 transducer (focal depth: 3 cm) was used to obtain *ex vivo* photoacoustic images. **(C)** *In vivo* PA images of metastasized lung clearly showed a PA signal was detected when I@C6-NPs were intravenously injected compared to I@NPs. VisualSonics Vevo LAZR-2100 device equipped with a 40-MHz transducer was used to obtain *in vivo* photoacoustic images. **(D)** PA signals inside the lung were quantified (ANOVA, $p<0.01$). **(E)** *Ex vivo* PA imaging of extracted lungs 6 h after the injection of I@NPs and I@C6-NPs. L7_4 transducer was used to obtain *ex vivo* photoacoustic images.

In addition, the CEACAM6-targeting nanomedicine inhibited the formation of metastasis *in vivo* more efficiently than did the non-targeting nanomedicine both in blood-circulating stage (**Figure 7**) and early-metastasized stage (**Figure S9**). These results highlight the versatility of the CEACAM6-targeting nanomedicine for the treatment of a variety of metastatic tumor types. In addition, a recent study indicated that therapeutic effect can be expected by increasing the anoikis sensitivity of lung adenocarcinoma using CEACAM6 monoclonal antibodies [16]. This further emphasizes the suitability of CEACAM6 as a metastatic tumor cell biomarker. Even though there is another application of CEACAM6 as a molecular target for imaging [28], this study is the first to develop a photoacoustics-based theranostic nanomedicine using CEACAM6 for the treatment of metastatic tumor cells.

In vivo, D@C6-NPs inhibited tumor metastasis successfully by delivering the chemotherapeutic agent to blood-circulating tumor cells efficiently (**Figure 7**). However, D@NPs inhibited metastasis to a lower extent compared with free DOX, in contrast with the results of *in vitro* experiments. This may be due to the inability of non-targeting drug delivery systems to treat blood-circulating metastatic tumor cells. Unlike the *in vitro* static condition (**Figure 6**), irregular and turbulent blood flow *in vivo* hinders the uptake of NPs into metastatic tumor cells, resulting in lower inhibition of metastasis by D@NPs compared with

that by free DOX *in vivo* (**Figure 7A-B**). The tHSA-NPs displayed insufficient targeting or uptake ability in the shaking condition (**Figure 5A**, row 3). In addition, the amount of chemotherapeutic agent (DOX) delivered by D@NPs was lower than that of free DOX in the shaking condition (**Figure S6**). Furthermore, therapies are conducted right after the intravenous injection of AR cells; therefore, the enhanced permeability and retention (EPR) effect cannot be expected. Thus, D@NPs showed limited therapeutic effect. However, C6-NPs were highly effective in their targeting or uptake ability in the same condition within a short period of time (30 min) via CEACAM6-mediated targeting (**Figure 5A**, row 4) and following endocytosis [29]. Consequently, D@C6-NPs showed excellent inhibition of metastatic tumor formation in blood-circulating AR tumor cells in the animal model.

Metastasis can occur through blood vessels and through the lymphatic system or by direct migration of tumor cells to adjacent tissues [30]. Therefore, the ability to target and treat early-stage metastatic tumors is important, in addition to targeting circulating metastatic tumor cells in the blood vessels. In the *in vitro* and *in vivo* studies, re-attached AR tumor cells were found to overexpress CEACAM6 (**Figure 4D** and **Figure S2B**) [31]. Thus, CEACAM6 can be an excellent biomarker targeting metastatic tumor cells in the early stage of metastasis as well as for tumor cells circulating in the blood. In addition to the metastatic tumor cell targeting ability of D@C6-NPs in the bloodstream, the efficient delivery of albumin NPs to solid tumors via the EPR effect and gp60-mediated transcytosis have been reported [32]. In this study, the blood vessels were found to be sufficiently developed in early-stage lung metastatic tumor colonies (**Figure S2A**). Therefore, circulating CEACAM6-targeting nanomedicines can be expected to be extravasated from the bloodstream into the metastatic tumor sites and target CEACAM6 biomarkers in the tumor cells. Therefore, CEACAM6-targeting HSA-based NPs have the potential to treat metastatic AR tumor cells in the bloodstream as well as early-stage metastatic tumors.

Photoacoustic imaging has several advantages of imaging early metastasized tumors, such as real-time performance, non-invasive nature, and high-resolution and functionalized imaging [17, 18]. Therefore, when combined with metastasis-specific contrast agents, photoacoustic imaging is the most suitable strategy for the effective and early diagnosis of metastasis at a lower cost than that of other imaging modalities, such as magnetic resonance imaging and computed tomography. The metastasized tumors were found to be neovascularized with the immunohistochemical analysis of CD31, which is a neovascularization factor [33] (**Figure S2A**). As a result, circulating nanomedicines could be expected to access the metastasized tumors through neovessels. In addition, re-attached AR cells in the metastasized tumors were found to continue overexpressing CEACAM6 biomarkers (**Figure S2B**). Therefore, the intravenously administered I@C6-NPs showed high photoacoustic signal intensities in the metastatic tumors. The photoacoustic image from extracted *ex vivo* metastasized lungs (**Figure 8E**) displayed a pattern of metastatic nodules shown in **Figure 7A**. Likewise, the results of real-time lung photoacoustic imaging demonstrated the ability of the nanomedicine to efficiently target metastatic tumors *in vivo* (**Figure 8**). Even though the photoacoustic signals of I@NPs (non-targeting nanomedicine) were also detected inside the lungs, they were indistinguishable from the background noise caused by the blood-circulating nanomedicine or natural photoacoustic substances, such as hemoglobin and melanin. On the other hand, I@C6-NPs (CEACAM6-targeting nanomedicine) showed clear photoacoustic signals inside the metastasized tumors in the lungs compared to the background noise (**Figure 8 and Figure S11**). In this study, the experiments focused only on lung metastasis. However, the detection of metastasis in other organs can be anticipated, considering the versatility of the CEACAM6-targeting strategy. In particular, direct imaging of circulating metastatic AR tumor cells in the bloodstream based on the high resolution of photoacoustic imaging might also be possible [34, 35].

In summary, a novel CEACAM6-targeting HSA-based nanomedicine has been developed to target circulating metastatic AR tumor cells and detect early-stage metastasized tumors. In both *in vitro* and *in vivo* studies, the nanomedicine efficiently delivered an encapsulated chemotherapeutic agent (DOX) to circulating metastatic AR tumor cells and successfully suppressed tumor metastasis. Furthermore, the albumin-based nanomedicine with intrinsic binding ability to ICG has great potential as a photoacoustic imaging agent to target metastatic tumor cells. Consequently, early-stage metastasized tumors can be successfully detected by photoacoustic imaging *in vivo*. In conclusion, this study demonstrated the potential benefits of the CEACAM6-targeting nanomedicine for the therapy and diagnosis of metastatic AR tumor cells.

Abbreviations

2-IT: 2-iminothiolane hydrochloride; AR: anoikis-resistance; CEACAM6: carcinoembryonic antigen-related cell adhesion molecule 6; DAPI:

4',6-diamidino-2-phenylindole; DOX: doxorubicin; EDC: 1-ethyl-3-(3-dimethylaminopropyl)carbodiimide; EDTA: ethylenediaminetetraacetic acid; EPR: enhanced permeability and retention; GSH: glutathione; HEPES: 4-(2-hydroxyethyl)-1-piperazine-ethanesulfonic acid; HPLC: high-performance liquid chromatography; HSA: human serum albumin; ICG: indocyanine green; NHS: N-hydroxysuccinimide; PA: photoacoustic; PFA: paraformaldehyde; poly-HEMA: poly(2-hydroxyethyl methacrylate); RT-PCR: reverse transcription polymerase chain reaction; tHSA-NPs: thiolated human serum albumin nanoparticles.

Acknowledgements

This work was supported by the Korea Health Industry Development Institute (KHIDI), funded by the Ministry of Health & Welfare (Grant Number: HI15C2797) and by the Basic Science Research Program through the National Research Foundation of Korea (NRF), funded by the Ministry of Education, Science and Technology (NRF-2016R1A6A1A0301 2845, and NRF-2017R1A2B2003194), Republic of Korea.

Supplementary Material

Supplementary figures.
http://www.thno.org/v08p4247s1.pdf

Competing Interests

The authors have declared that no competing interest exists.

References

1. Mehlen P, Puisieux A. Metastasis: a question of life or death. Nat Rev Cancer. 2006; 6: 449-58.
2. Kerbel RS, Kobayashi H, Graham CH. Intrinsic or acquired drug-resistance and metastasis - are they linked phenotypes. J Cell Biochem. 1994; 56: 37-47.
3. Voulgari A, Pintzas A. Epithelial-mesenchymal transition in cancer metastasis: Mechanisms, markers and strategies to overcome drug resistance in the clinic. Biochim Biophys Acta. 2009; 1796: 75-90.
4. Lee K, Lee H, Bae KH, Park TG. Heparin immobilized gold nanoparticles for targeted detection and apoptotic death of metastatic cancer cells. Biomaterials. 2010; 31: 6530-6.
5. Yang F, Jin C, Yang D, Jiang YJ, Li J, Di Y, et al. Magnetic functionalised carbon nanotubes as drug vehicles for cancer lymph node metastasis treatment. Eur J Cancer. 2011; 47: 1873-82.
6. Liang C, Diao S, Wang C, Gong H, Liu T, Hong GS, et al. Tumor metastasis inhibition by imaging-guided photothermal therapy with single-walled carbon nanotubes. Adv Mater. 2014; 26: 5646.
7. O'Brien MER, Wigler N, Inbar M, Rosso R, Grischke E, Santoro A, et al. Reduced cardiotoxicity and comparable efficacy in a phase III trial of pegylated liposomal doxorubicin HCl (CAELYX (TM)/Doxil (R)) versus conventional doxorubicin for first-line treatment of metastatic breast cancer. Ann Oncol. 2004; 15: 440-9.
8. Lee H, Park S, Kim JB, Kim J, Kim H. Entrapped doxorubicin nanoparticles for the treatment of metastatic anoikis-resistant cancer cells. Cancer Lett. 2013; 332: 110-9.
9. Simpson CD, Anyiwe K, Schimmer AD. Anoikis resistance and tumor metastasis. Cancer Lett. 2008; 272: 177-85.
10. Duxbury MS, Ito H, Zinner MJ, Ashley SW, Whang EE. CEACAM6 gene silencing impairs anoikis resistance and in vivo metastatic ability of pancreatic adenocarcinoma cells. Oncogene. 2004; 23: 465-73.
11. Blumenthal RD, Hansen HJ, Goldenberg DM. Inhibition of adhesion, invasion, and metastasis by antibodies targeting CEACAM6 (NCA-90) and CEACAM5 (Carcinoembryonic Antigen). Cancer Res. 2005; 65: 8809-17.
12. Duxbury MS, Matros E, Clancy T, Bailey G, Doff M, Zinner MJ, et al. CEACAM6 is a novel biomarker in pancreatic adenocarcinoma and PanIN lesions. Annals of surgery. 2005; 241: 491.
13. Ieta K, Tanaka F, Utsunomiya T, Kuwano H, Mori M. CEACAM6 gene expression in intrahepatic cholangiocarcinoma. Br J Cancer. 2006; 95: 532-40.
14. Lewis-Wambi JS, Cunliffe HE, Kim HR, Willis AL, Jordan VC. Overexpression of CEACAM6 promotes migration and invasion of oestrogen-deprived breast cancer cells. Eur J Cancer. 2008; 44: 1770-9.
15. Niu G, Murad YM, Gao HK, Hu S, Guo N, Jacobson O, et al. Molecular targeting of CEACAM6 using antibody probes of different sizes. J Control Release. 2012; 161: 18-24.
16. Hong KP, Shin MH, Yoon S, Ji GY, Moon YR, Lee OJ, et al. Therapeutic effect of anti CEACAM6 monoclonal antibody against lung adenocarcinoma by enhancing anoikis sensitivity. Biomaterials. 2015; 67: 32-41.
17. Moon H, Kang J, Sim C, Kim J, Lee H, Chang JH, et al. Multifunctional theranostic contrast agent for photoacoustics-and ultrasound-based tumor diagnosis and ultrasound-stimulated local tumor therapy. J Control Release. 2015; 218: 63-71.
18. Moon H, Kumar D, Kim H, Sim C, Chang J-H, Kim J-M, et al. Amplified photoacoustic performance and enhanced photothermal stability of reduced graphene oxide coated gold nanorods for sensitive photoacoustic imaging. ACS nano. 2015; 9: 2711-9.
19. Moody ED, Viskari PJ, Colyer CL. Non-covalent labeling of human serum albumin with indocyanine green: a study by capillary electrophoresis with diode laser-induced fluorescence detection. J Chromatogr B. 1999; 729: 55-64.
20. Niknejad H, Mahmoudzadeh R. Comparison of different crosslinking methods for preparation of docetaxel-loaded albumin nanoparticles. Iran J Pharm Res. 2015; 14: 385-94.
21. Yang F, Zhang Y, Liang H. Interactive association of drugs binding to human serum albumin. Int J Mol Sci. 2014; 15: 3580-95.
22. Son S, Song S, Lee SJ, Min S, Kim SA, Yhee JY, et al. Self-crosslinked human serum albumin nanocarriers for systemic delivery of polymerized siRNA to tumors. Biomaterials. 2013; 34: 9475-85.
23. Mihl C, Wildberger JE, Jurencak T, Yanniello MJ, Nijssen EC, Kalafut JF, et al. Intravascular enhancement with identical iodine delivery rate using different iodine contrast media in a circulation phantom. Invest Radiol. 2013; 48: 813-8.
24. Visvader JE, Lindeman GJ. Cancer stem cells in solid tumours: accumulating evidence and unresolved questions. Nat Rev Cancer. 2008; 8: 755-68.
25. Nagaprashantha LD, Vatsyayan R, Lelsani PCR, Awasthi S, Singhal SS. The sensors and regulators of cell–matrix surveillance in anoikis resistance of tumors. Int J Cancer. 2011; 128: 743-52.
26. Zhao ZS, Li L, Wang HJ, Wang YY. Expression and prognostic significance of CEACAM6, ITGB1, and CYR61 in peripheral blood of patients with gastric cancer. J Surg Oncol. 2011; 104: 525-9.
27. Jantscheff P, Terracciano L, Lowy A, Glatz-Krieger K, Grunert F, Micheel B, et al. Expression of CEACAM6 in resectable colorectal cancer: a factor of independent prognostic significance. J Clin Oncol. 2003; 21: 3638-46.
28. Zaman MB, Baral TN, Jakubek ZJ, Zhang JB, Wu XH, Lai E, et al. Single-domain antibody bioconjugated near-IR quantum dots for targeted cellular imaging of pancreatic cancer. J Nanosci Nanotechno. 2011; 11: 3757-63.
29. Choi CHJ, Hao LL, Narayan SP, Auyeung E, Mirkin CA. Mechanism for the endocytosis of spherical nucleic acid nanoparticle conjugates. Proc Natl Acad Sci U S A. 2013; 110: 7625-30.
30. Declerck YA, Perez N, Shimada H, Boone TC, Langley KE, Taylor SM. Inhibition of invasion and metastasis in cells transfected with an inhibitor of metalloproteinases. Cancer Res. 1992; 52: 701-8.
31. Blumenthal RD, Leon E, Hansen HJ, Goldenberg DM. Expression patterns of CEACAM5 and CEACAM6 in primary and metastatic cancers. BMC cancer. 2007; 7: 2.
32. Sim C, Kim H, Moona H, Lee H, Chang JH, Kim H. Photoacoustic-based nanomedicine for cancer diagnosis and therapy. J Control Release. 2015; 203: 118-25.
33. Shah F, Balan P, Weinberg M, Reddy V, Neems R, Feinstein M, et al. Contrast-enhanced ultrasound imaging of atherosclerotic carotid plaque neovascularization: a new surrogate marker of atherosclerosis? Vasc Med. 2007; 12: 291-7.
34. Galanzha EI, Shashkov EV, Kelly T, Kim JW, Yang LL, Zharov VP. In vivo magnetic enrichment and multiplex photoacoustic detection of circulating tumour cells. Nat Nanotechnol. 2009; 4: 855-60.

35. Mallidi S, Luke GP, Emelianov S. Photoacoustic imaging in cancer detection, diagnosis, and treatment guidance. Trends Biotechnol. 2011; 29: 213-21.